Asian Journal of Chemistry; Vol. 32, No. 2 (2020), 265-270

ASIAN JOURNAL OF CHEMISTRY

https://doi.org/10.14233/ajchem.2020.22306

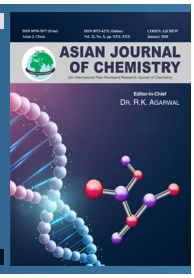

Magnetic, Thermal and Electrical Transport Properties of *o*-Substituted Polyanilines Encapsulated with Fe_2O_3 Nanoparticles

R. Suganthi, S. Padmaja and S. Jhancy Mary*

Department of Chemistry, Auxilium College (Autonomous), Vellore-632006, India

*Corresponding author: Fax: +91 416 2247281; E-mail: jhancy2011@gmail.com

Received: 1 July 2019; *Accepted*: 9 August 2019; *Published online*: 30 December 2019; AJC-19710

Poly(2-nitroaniline), poly(2-nitroaniline)-Fe_2O_3 and poly(2-methylaniline)-Fe_2O_3 nanocomposites synthesized by *in situ* chemical oxidative polymerization technique were characterized by XRD, thermal (TGA and DTA) and FTIR & UV-visible spectroscopic techniques. The thermal stability was confirmed by the integral procedural decomposition temperature (IPDT) and oxidation index (OI) calculations. The electrical conductivity and dielectric properties were also investigated. At low frequency region, the dielectric constant decreases with increase in frequency due to electrical relaxation process. At high frequencies, dielectric constant is independent of frequency. At low frequency, there was strong frequency dispersion of permittivity and above 3 Hz, a frequency independent behaviour in permittivity was observed. The materials exhibit ferromagnetic behaviour.

Keywords: Nanocomposites, Oxidative polymerization, Electrical conductivity, Dielectric, Ferromagnetic.

INTRODUCTION

Conducting polymers are rapidly gaining attraction with improved processable materials having unique electrical, electrochemical and optical properties [1,2]. Polymeric nanocomposites (PNCs) containing nanosized metal oxides are under extensive research, since they exhibit exciting characteristics with unique applications such as quantum electronic devices, magnetic recording materials, sensors, capacitors, smart windows, toners in photocopying, conducting paints and rechargeable batteries [3-7]. However, due to poor mechanical properties, they cannot be processed easily [8-10]. By combining conducting polymers with metal oxide nanoparticles, one could produce polymeric nanocomposites, the properties of which can be fine-tuned depending on the composition of metal oxide in polymer matrix. Nanocomposites of polyaniline (PANI) have been widely studied [11-15] due to their unique electrical, dielectrical, optical and optoelectrical properties.

Nanocomposites demonstrate significant improvements in mechanical strength, toughness, electrical and thermal conductivity [16]. The combination of organic and inorganic precursors makes it possible to enhance their thermal and chemical stabilities. The synthesis of polymeric inorganic composite has received a great deal of attention because it provides new materials with special mechanical, chemical, electrochemical and optical as well as magnetic properties [17]. Various morphologies of polyaniline and its nanocomposites including nanowires [18], nanofibers [19], nanospheres [20] and nanosheets [21,22] have been widely explored.

In this work, we report the thermal, magnetic and electrical transport properties of the chemically synthesized and characterized poly(2-nitroaniline), poly(2-nitroaniline-Fe_2O_3 and poly(2-methylaniline-Fe_2O_3 nanocomposite. An attempt has been made to understand and compare the influence of Fe_2O_3 on the magnetic properties, dielectric properties, impedance and electrical conductivity of synthesized nanocomposite. The frequency dependence of dielectric constant, dielectric loss, imaginary modulus, real modulus and tan δ are discussed. Complex impedance spectroscopic study was made for understanding the charge transport mechanism [23,24]. The frequency dependent conductivity and dielectric permittivity provide information on the electronic transport mechanism. It reflects the presence of disorder in the molecular structure of the materials and the process of electrical transport [24].

EXPERIMENTAL

2-Nitroaniline, ammonium persulphate and sodium dodecyl sulfate (SDS) surfactant were purchased from LOBA Chemic, Qualigens and Avra Synthesis Pvt. Ltd., respectively. Fe_2O_3 (gamma) nanoparticles were purchased from SRL.

Characterization techniques: FT-IR measurements have been carried out using IRAffinity-1 Fourier transform infrared spectrophotometer (Shimadzu) in the wavenumber range 4000-500 cm^{-1}. The UV-visible analyses were carried out using Perkin-Elmer Lambda double beam spectrophotometer in the wavelength range 200-800 nm. XRD analyses were performed on a Bruker AXS D8 advance using Cu as X-ray source at the wavelength of 1.5406 Å of angular range from 3º to 135º. Thermogravimetric analyses were carried out with a Perkin-Elmer STA 6000 from room temperature to 700 ºC under inert gas atmosphere. Dielectric constants were measured by NOVO CONTROL technologies GmbH and Co, Germany. Electrical conductivity measurements were made using German model concept 80 in the frequency range from 10 Hz to 1 MHz at room temperature. Z″ *versus* Z′ complex impedance plots were plotted for the nanocomposites and the bulk resistance (R_b) was evaluated by analyzing the impedance data using ZSimp Demo software. Vibrating sample magnetometer, LAKESHORE VSM 7410 was used to study the magnetic properties.

***in situ* Chemical synthesis by oxidative polymerization:** Poly(2-nitroaniline) ($P2NO_2Ani$), poly(2-nitroaniline)-Fe_2O_3 ($P2NO_2Ani/Fe_2O_3$) and poly(2-methylaniline)-Fe_2O_3 (P2MeAni/Fe_2O_3) have been chemically synthesized by *in situ* chemical oxidative technique with ammonium persulphate as initiator, hydrochloric acid as dopant and sodium lauryl sulphate (SDS) as an emulsifier. 2-Nitroaniline (6.9 mL) was mixed with 0.1 M (1.44 g/50 mL) SDS in a glass beaker and stirred under ice cold conditions. Ammonium persulphate (0.2 mol, 100 mL) and HCl (1M , 100 mL) were taken in a separate beakers. The acid and initiator were added dropwise to the monomer for a period of 4 h with constant stirring. The mixture was stirred for another 2 h, kept at 0 ºC overnight, filtered, washed with deionized water and dried. The dried polymer was then suspended in 100 mL of deionized water and stirred on a magnetic stirrer for 2 h. Filtered, washed with deionized water and finally with few drops of methanol, dried and powdered. The Fe_2O_3 nanocomposites were also synthesized adopting the same procedure by adding Fe_2O_3 nanoparticles along with the monomer initially. The composites were soluble in DMSO, DMF and partially soluble in toluene and chloroform. Table-1 presents the yield percentage of the synthesized materials.

TABLE-1
YIELD (%) OF THE NANOCOMPOSITES

Polymer nanocomposites	Yield (%)
$P2NO_2Ani$	58.32
$P2NO_2Ani$-Fe_2O_3	47.15
P2MeAni- Fe_2O_3	94.40

RESULTS AND DISCUSSION

FT-IR analysis: Infrared spectrum of P2NO2Ani (Fig. 1a) shows absorption peaks around 3473 and 1340 cm^{-1} due to -N-H and C-N stretching of the secondary amine, respectively. The peaks at 1566 and 1496 cm^{-1} are assigned to the -C=C- stretching frequencies of quinonoid and benzenoid rings and can also be ascribed to asymmetric and symmetric stretching vibration in NO_2 group. The peak at 1166 cm^{-1} is due to the electrical conductivity band [25].

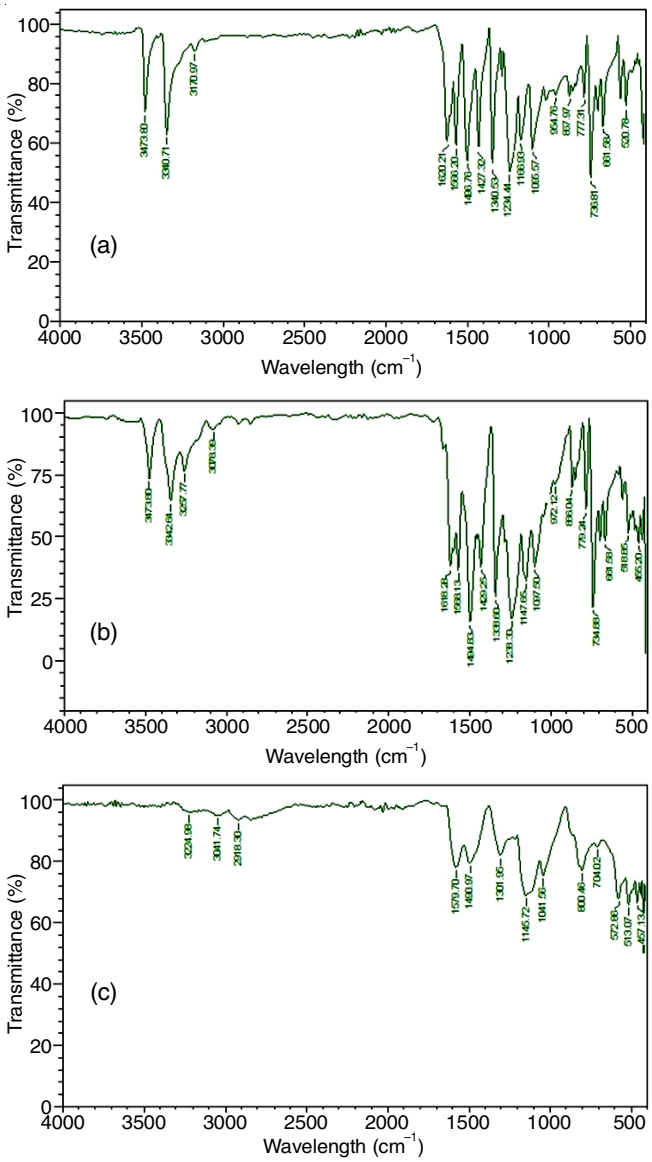

Fig. 1. FTIR spectra of $P2NO_2Ani$ (a), $P2NO_2Ani$-Fe_2O_3 (b) and P2MeAni-Fe_2O_3 (c)

The C-H out of plane bending vibration of 1,2,4-tri substituted benzene rings appear around at 954 and 800 cm^{-1}. The band at 736 cm^{-1} corresponds to in-plane bending of C-NO_2 [26]. The electrical conductivity band confirms the formation of emeraldine salt form.

The spectrum of $P2NO_2Ani$-Fe_2O_3 shows absorption peaks at 3473 and 1338 cm^{-1} due to -N-H and C-N stretching of 2º amine, respectively (Fig. 1b). The main peaks at 1568 and 1494 cm^{-1} correspond to quinone and benzene ring deformations, respectively. The peak at 518 cm^{-1} is due to metal-oxygen stretching vibration (Fe-O). It confirms the presence of Fe_2O_3 nanoparticles on the polymer chains. The peak at 1338 cm^{-1} is due

to nitro group. The peaks at 972 and 866 cm^{-1} are characteristic of 1,2,4-tri substituted aromatic rings. The peak at 1147 cm^{-1} is due to the electrical conductivity band. The peak at 734 cm^{-1} corresponds to in-plane bending of C-NO_2 group.

The infrared spectrum of P2MeAni-Fe_2O_3 (Fig. 1c) shows the absorption peaks around 3224 and 1301 cm^{-1} due to -N-H and C-N stretchings, respectively. The peaks at 1579 and 1490 cm^{-1} are assigned to the -C=C- stretching frequencies of quinonoid and benzenoid rings. The peak at 572 cm^{-1} confirms the incorporation of Fe_2O_3 nanoparticles into the polymer chains. The peak at 1145 cm^{-1} is due to the electrical conductivity band. Moreover, the peaks at 3041 and 2918 cm^{-1} are due to asymmetric and symmetric stretching vibrations of C-H bonds present in methyl groups.

UV-Visible analysis: Fig. 2a shows the absorption spectrum of P2NO_2Ani dissolved in DMSO. The UV absorption band at 210 nm is due to the π-π* transition. The band at 290 nm is due to n-π* transition. The n-π* transition is due to the transition of lone pair of electrons of nitrogen atoms to an empty non bonding molecular orbital.

The absorption spectrum of nitroaniline composite is shown in Fig. 2b. It shows major absorptions around 260 nm due to π-π* transition on the polymer chains and the absorption around 350 nm is due to the n-π* transition of quinonoid rings and corresponds to the localization of electrons [27]. The polaron band appears around 410 nm. When compared to p2NO_2Ani, p2NO_2Ani-Fe_2O_3 nanocomposite absorbs at higher wavelength. The red shift is observed in the polymer composite, which confirms the encapsulation of ferric oxide nanoparticles.

The absorption spectrum of P2MeAni/Fe_2O_3 (Fig. 2c) shows major absorptions around 260 nm due to π-π* transition on the polymer chains and the absorption around 325 nm is due to the n-π* transition of quinonoid rings and corresponds to the localization of electrons [27]. The polaron band appears around 445 nm.

XRD analysis: The XRD patterns of poly(2-nitroaniline) polymer shows the sharp diffraction peaks due to the crystalline nature (Fig. 3a). P2MeAni-Fe_2O_3 composite shows a broad diffraction peak around at 2θ =25º and 43º due to the characteristic peaks of emeraldine salt structure (Fig. 3b) but the composite exhibits amorphous nature.

Thermogravimetric analysis: The TGA of P2NO_2Ani shows three steps weight loss. The first weight loss is due to loss of water and moisture (Fig. 4a). The second weight loss up to 250 ºC (5.659 % loss) is due to removal of dopant molecules. The third step (2.965 %) decomposition of composite takes place around 450 ºC. The polymer composite leaves some char content (17.41 %), which is due to ferric oxide nanoparticles.

TGA of P2MeAni-Fe_2O_3 nanocomposite also exhibits a three-steps weight loss. At first, a weight loss (8.738 %) is due to loss of water and moisture which takes place around 100 ºC. The second weight loss upto 575 ºC, (44.41 %) is due to the removal of dopant molecules. In the third step, weight loss of 5.266 % is due to decomposition of composite (Fig. 4b).

Integral procedural decomposition temperature (IPDT) is a useful parameter for assessing the overall thermal stability of the polymers during the decomposition process. The area was calculated using the following equations:

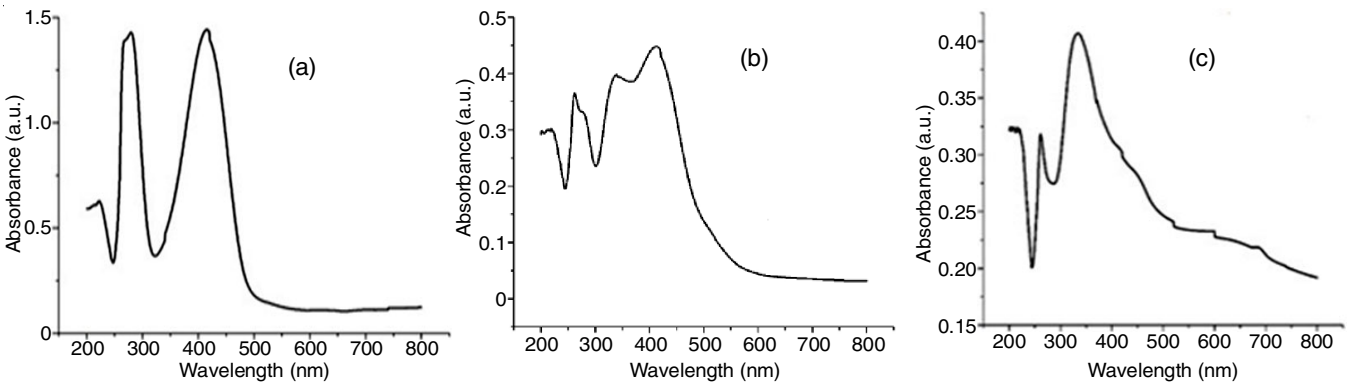

Fig. 2. UV-Visible spectra of P2NO_2Ani (a), P2NO_2Ani-Fe_2O_3 (b) and P2MeAni-Fe_2O_3 (c)

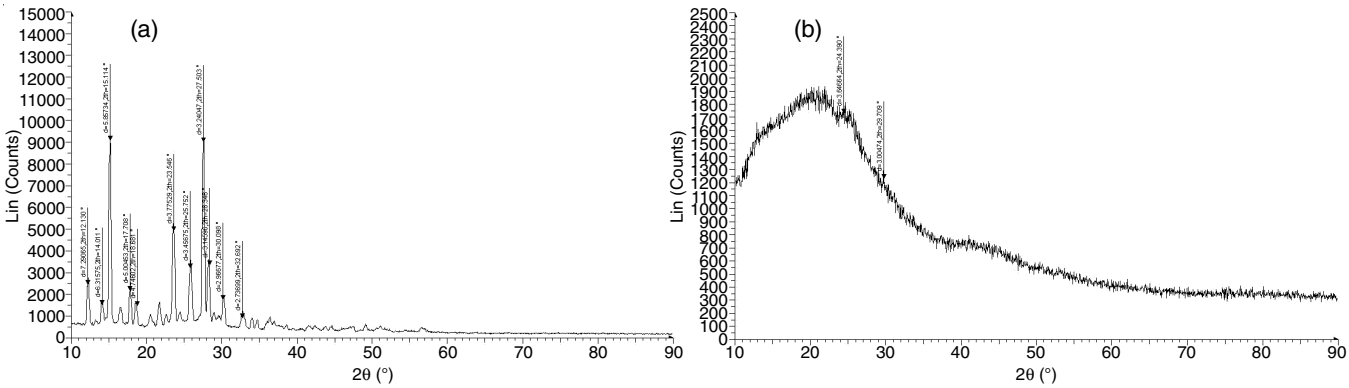

Fig. 3. XRD spectra of P2NO_2Ani (a) and P2MeAni-Fe_2O_3 (b)

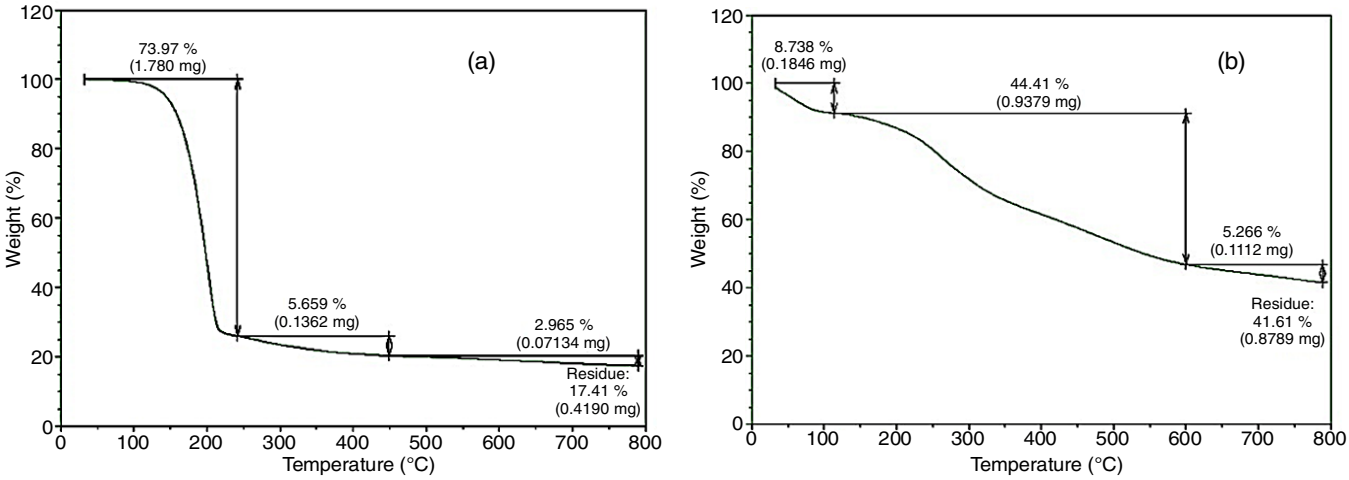

Fig. 4. Thermograms of P2NO$_2$Ani (a) and P2MeAni-Fe$_2$O$_3$ (b)

$$IPDT\ (°C) = A \times K \times (T_f - T_i)$$

$$A = \frac{S_1 + S_2}{S_1 + S_2 + S_3}$$

$$K = \frac{S_1 + S_2}{S_1}$$

where A is the area ratio of total experimental curve defined by the total TGA thermogram, K is the coefficient, T_i and T_f are the initial and final experimental temperatures, respectively in ºC. The oxidation index (OI) was calculated from the weight of carbon residue, which is related to flame retardant capacity of composites [28] and the values are tabulated in Table-2.

$$OI \times 100 = 17.5 \times 0.4\ CR$$

The P2MeAni-Fe$_2$O$_3$ nanocomposite is thermally more stable than pNO$_2$Ani, where sulphonate anions give more rigidity to the polymer chains that resists the thermal degradation.

TABLE-2
IPDT AND OI VALUES OF THE
POLYMER AND NANOCOMPOSITES

Polymer/nanocomposite	IPDT	OI
P2NO$_2$Ani	416	0.0293
P2MeAni-Fe$_2$O$_3$	473	0.0614

Electrical transport properties: Total electrical conductivity (σ) values have been calculated using the formula, $\sigma = t/R_bA$ where t is the thickness of pellet, A is the area covered by silver electrodes in contact with the material and R_b is the bulk resistance of material. The ZSimp Demo software has been used to get the value of bulk resistance from the intercept on the real axis at the high frequency portion of Nyquist plots. The electrical conductivity values are tabulated in Table-3.

TABLE-3
ELECTRICAL CONDUCTIVITY VALUES OF
THE POLYMER AND NANOCOMPOSITE

Polymer/ nanocomposite	Thickness	R_b	Conductivity (S cm^{-1})
P2NO$_2$Ani	0.94	7.20×10^5	1.66×10^{-6}
P2MeAni-Fe$_2$O$_3$	0.77	8.23×10^5	2.66×10^{-6}

At high frequencies, these plots exhibit semi-circular arcs due to the bulk properties. The conductivity values are of the order of 10^{-6} in the semiconducting range.

Dielectric properties: Fig. 5 shows the plot of dielectric constant *versus* frequency. The dielectric constant of P2MeAni Fe$_2$O$_3$ decreases with increase in frequency in the low frequency region due to electrical relaxation process. High dielectric permittivity at low frequency region is due to space charge polarization due to the presence of free charges at the interface [29]. At high frequencies, dielectric constant is independent of frequency as it remains almost constant. At low frequency there is a strong frequency dispersion of permittivity and above 3 Hz it is independent of frequency. In case of P2NO$_2$Ani, dielectric constant is independent of frequency which is attributed due to electron withdrawing nature of nitro group, which decreases the electron density along the polymer chain.

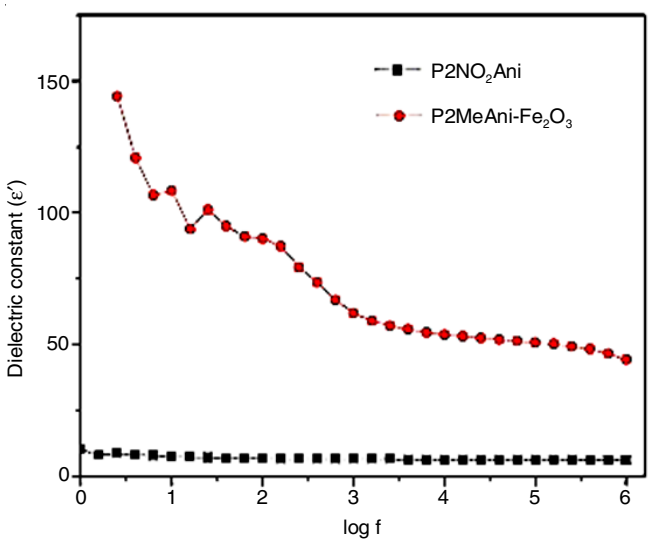

Fig. 5. Plots of dielectric constant with frequency

Dielectric loss is a measure of energy dissipated and generally comprises of the contribution from ionic transport as well as polarization of a charge or dipole. In Fig. 6, dielectric loss is high in -CH$_3$ substituted polyaniline nanocomposite due to free charge motion within the material, a phenomenon leading to conductivity relaxation [30]. Dielectric loss decreases with

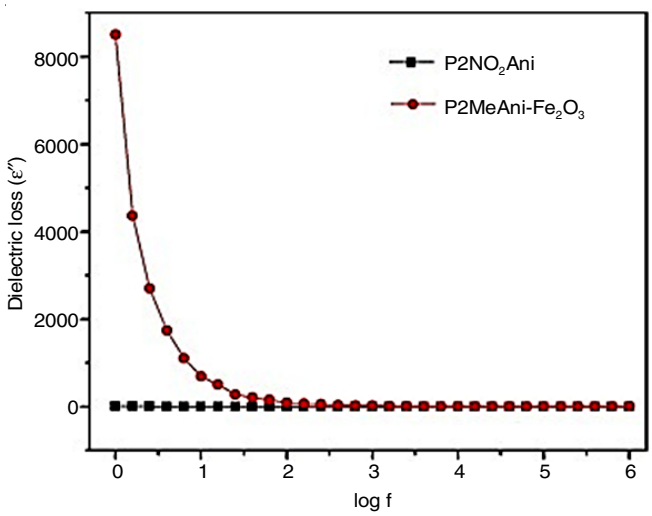

Fig. 6. Plots of dielectric loss with frequency

increases in frequency upto 2 Hz. This is due to the free movement of the charges in polymer matrix. On increasing the frequency upto 6 Hz, there is no change in dielectric loss as it almost remains constant. In $P2NO_2Ani$ polymer, dielectric loss is independent of frequency.

The variation of dielectric modulus, real and imaginary parts with frequency are given in Fig. 7, respectively. The real part of modulus spectra increases with increasing frequency. The imaginary part of dielectric modulus spectra increases up to a certain frequency followed by decreasing trend with increasing frequency. In this case, electrode polarization/interfacial polarization effect is seen to be completely vanishing in contrast to the dielectric formalism. The appearance of a peak in imaginary part of the dielectric modulus in $P2NO_2Ani$ can be assumed to be related with the translation ionic dynamics and the conductivity relaxation of the mobile ions [31].

Fig. 8 shows the plot of tan δ with frequency. In P2MeAni /Fe_2O_3 tan δ increases with increase in frequency upto 2 Hz due to the presence of relaxing dipolar. When frequency greater than 2 Hz is applied tan δ does not vary much with frequency and this is attributed to non-relaxation dipole. A frequency independent behaviour is observed in $p2NO_2Ani$ polymer.

Magnetic properties: In order to investigate the magnetic properties of P2MeAni-Fe_2O_3 composite, a VSM analysis was also performed (Fig. 9). P2MeAni-Fe_2O_3 nanocomposite exhibits hysteresis loop and hence it is ferromagnetic. The magnetic saturation is seen at 0.75 emu/g.

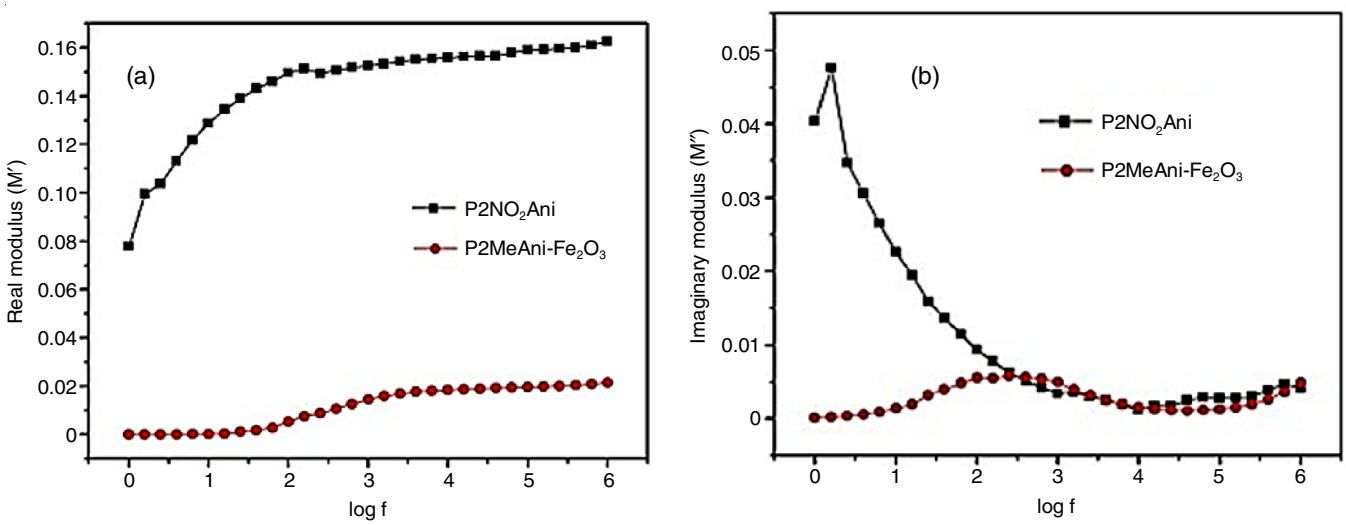

Fig. 7. Plots of real modulus (a) and imaginary modulus (b) with frequency

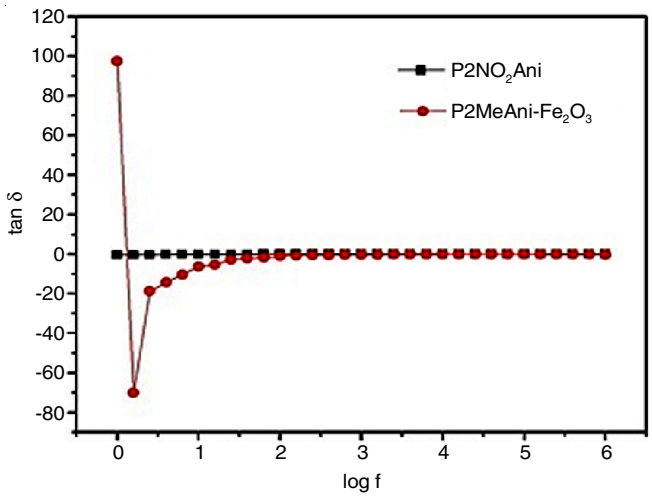

Fig. 8. Plots of tan δ with frequency

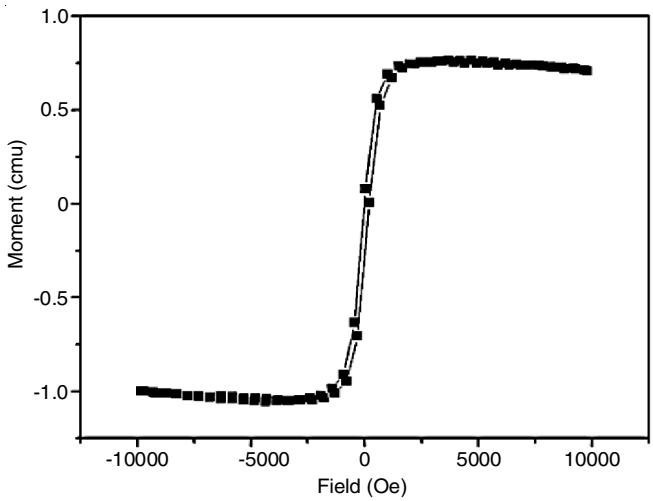

Fig. 9. Magnetic properties of P2MeAni-Fe_2O_3

Conclusion

in situ Chemical oxidative polymerization was performed in the presence of host material, Fe_2O_3 to synthesize P2NO_2Ani-Fe_2O_3 andP2MeAni-Fe_2O_3 nanocomposites. The NO_2 substituted polymer was also prepared. Spectroscopic results confirm the inclusion of Fe_2O_3 nanoparticles into the -NO_2 and -CH_3 substituted polyaniline chains. Thermogravimetric results confirmed the thermal stability of the nanocomposites. The conductivities as measured by four probe technique were of the order of 10^{-6} S cm^{-1}. The conductivity values are in the range of semiconductors. These materials will have a significant role to play as energy storage devices.

CONFLICT OF INTEREST

The authors declare that there is no conflict of interests regarding the publication of this article.

REFERENCES

1. A.O. Patil, A.J. Heeger and F. Wudl, *Chem. Rev.*, **88**, 183 (1988); https://doi.org/10.1021/cr00083a009.
2. K. Keiichi, Y. Katsumi and I. Yoshio, *Jpn. J. Appl. Phys.*, **21**, 567 (1982); https://doi.org/10.1143/JJAP.21.567.
3. Y. Wang, X. Wang, J. Li, J. Mo, X. Zhao, X. Jing and F. Wang, *Adv. Mater.*, **13**, 1582 (2001); https://doi.org/10.1002/1521-4095(200110)13:20<1582::AID-ADMA1582>3.0.CO;2-J.
4. G. Wegner and J. Rühe, *J. Farad. Discuss.*, **88**, 333 (1989); https://doi.org/10.1039/DC9898800333.
5. S. Roth and W. Graupner, *Synth. Met.*, **57**, 3623 (1993); https://doi.org/10.1016/0379-6779(93)90487-H.
6. M. Sato, S. Tanaka and K. Kaeriyama, *J. Chem. Soc. Chem. Commun.*, **11**, 873 (1986); https://doi.org/10.1039/c39860000873.
7. K.Y. Jen, R. Oboddi and R.L. Elsenbaumer, *Polym. Mater. Sci. Eng.*, **53**, 79 (1985).
8. D.R. Gagnon, J.D. Capistran, F.E. Karasz and R.W. Lenz, *Polym. Bull.*, **12**, 293 (1984); https://doi.org/10.1007/BF00263141.
9. R.B. Bjorklund and B. Liedberg, *J. Chem. Soc. C*, **16**, 1293 (1986); https://doi.org/10.1039/c39860001293.
10. M.-A. De Paoli, R.J. Waltman, A.F. Diaz and J. Bargon, *Polym. Sci. Polym. Chem.*, **23**, 1687 (1985); https://doi.org/10.1002/pol.1985.170230610.
11. S.E. Lindsey and G.B. Street, *Synth. Met.*, **10**, 67 (1984); https://doi.org/10.1016/0379-6779(84)90080-8.
12. A. Bozkurt, U. Akbulut and L. Toppare, *Synth. Met.*, **82**, 41 (1996); https://doi.org/10.1016/S0379-6779(97)80007-0.
13. C.M. Leu, Z.W. Wu and K.H. Wei, *Chem. Mater.*, **14**, 3016 (2002); https://doi.org/10.1021/cm0200240.
14. J. Wang, J. Yang, J. Xie and N. Xu, *Adv. Mater.*, **14**, 963 (2002); https://doi.org/10.1002/1521-4095(20020705)14:13/14<963::AID-ADMA963>3.0.CO;2-P.
15. L.H. Jiang, C.M. Leu and K.H. Wei, *Adv. Mater.*, **14**, 426 (2002); https://doi.org/10.1002/1521-4095(20020318)14:6<426::AID-ADMA426>3.0.CO;2-O.
16. M. Hughes, M.S. Shaffer, P.A.C. Renouf, C. Singh, G.Z. Chen, D.J. Fray and A.H. Windle, *Adv. Mater.*, **14**, 382 (2002); https://doi.org/10.1002/1521-4095(20020304)14:5<382::AID-ADMA382>3.0.CO;2-Y.
17. T. Vossmeyer, B. Guse, I. Besnard, R.E. Bauer, K. Mullen and A. Yasuda, *Adv. Mater.*, **14**, 238 (2002); https://doi.org/10.1002/1521-4095(20020205)14:3<238::AID-ADMA238>3.0.CO;2-#.
18. L. Liang, J. Liu, C.F. Windisch Jr., G.J. Exarhos and Y. Lin, *Angew. Chem. Int. Ed.*, **41**, 3665 (2002); https://doi.org/10.1002/1521-3773(20021004)41:19<3665::AID-ANIE3665>3.0.CO;2-B.
19. J. Huang, S. Virji, B.H. Weiller and R.B. Kaner, *J. Am. Chem. Soc.*, **125**, 314 (2003); https://doi.org/10.1021/ja028371y.
20. X. Guo, G.T. Fei, H. Su and L.D. Zhang, *Mat. Chem. J.*, **21**, 8618 (2011); https://doi.org/10.1039/c0jm04489j.
21. C. Zhou, J. Han and R. Guo, *Macromolecules*, **41**, 6473 (2008); https://doi.org/10.1021/ma800500u.
22. H. Zhang, J. Wang, Z. Wang, F. Zhang and S. Wang, *Macromol. Rapid Commun.*, **30**, 1577 (2009); https://doi.org/10.1002/marc.200900228.
23. R.P. Mc Call, E.M. Scherr, A.G. MacDiarmid and A. Epstein, *Phys. Rev. B*, **50**, 5094 (1994); https://doi.org/10.1103/PhysRevB.50.5094.
24. A.G. MacDiarmid and A.J. Epstein, *Macromol. Symp.*, **51**, 11 (1991); https://doi.org/10.1002/masy.19910510104.
25. J. Tang, X. Jing, B. Wang and F. Wang, *Synth. Met.*, **24**, 231 (1988); https://doi.org/10.1016/0379-6779(88)90261-5.
26. M.B. Wasu and A.R. Raut, *Int. J. Chem. Sci.*, **13**, 1285 (2015).
27. L.H.C. Mattoso, S.K. Manohar, A.G. MacDiarmid and A.J. Epstein, *J. Polym. Sci. A Polym. Chem.*, **33**, 1227 (1995); https://doi.org/10.1002/pola.1995.080330805.
28. S. Pashaei, S. Siddaramaiah, M. Avval and A. Syed, *Chem. Ind. Chem. Eng. Q.*, **17**, 141 (2011); https://doi.org/10.2298/CICEQ101007064P.
29. H.M. Kim, C.Y. Lee and J. Joo, *J. Korean Phys. Soc.*, **36**, 371 (2000).
30. J. Malathi, M. Kumaravadivel, G.M. Brahmanandhan, M. Hema, R. Baskaran and S. Selvasekarapandian, *J. Non-Cryst. Solids*, **356**, 2277 (2010); https://doi.org/10.1016/j.jnoncrysol.2010.08.011.
31. M. Hashim, Alimuddin, S.E. Shirsath, R.K. Kotnala, S.S. Meena, S. Kumar, A. Roy, R.B. Jotania, P. Bhatt and R. Kumar, *J. Alloys Compd.*, **573**, 198 (2013); https://doi.org/10.1016/j.jallcom.2013.03.029.